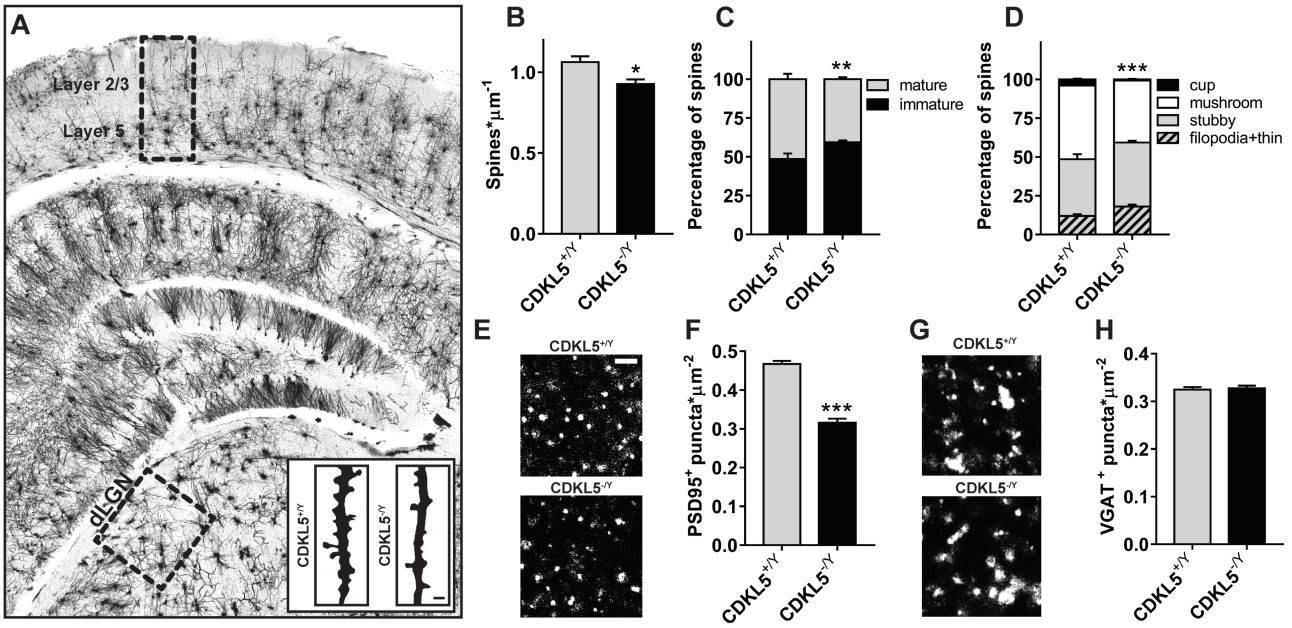

Figure 2. Morphological synaptic abnormalities in CDKL5 KO dLGN. **(A)** Representative image of a Golgi-stained coronal section containing the dLGN and showing the cortical layering that has been used in sections containing V1. **(B)** Quantitation of spine density in Golgi-stained dLGN slices showing a reduction in CDKL5$^{-/y}$ mice (two-tailed Student's *t*-test $P = 0.0259$). **(C)** Quantitation of the relative proportion of mature and immature spines in Golgi-stained dLGN slices showing an increased fraction of immature spines in CDKL5$^{-/y}$ mice (χ^2 test $P = 0.0027$). **(D)** Quantitation of spine morphology in Golgi-stained dLGN slices showing a pattern of decreased morphological maturity in CDKL5$^{-/y}$ mice (χ^2 test $P = 0.0009$). **(E)** Representative images of PSD95 punctate staining from CDKL5$^{-/y}$ and CDKL5$^{+/y}$ dLGN. **(F)** Quantitation of PSD95^{+} puncta density showing a reduction in CDKL5$^{-/y}$ mice (two-tailed Student's *t*-test $P < 0.0001$). **(G)** Representative images of VGAT punctate staining from CDKL5$^{-/y}$ and CDKL5$^{+/y}$ dLGN. **(H)** Quantitation of VGAT^{+} puncta density showing no difference in CDKL5$^{-/y}$ mice (two-tailed Student's *t*-test $P = 0.706$). *$P < 0.05$; **$P < 0.01$; ***$P < 0.001$. Scale bars (A, insets) are equal to 1 µm; (E and G), 2 µm. Error bars represent SEM.

results (27). Interestingly, we also found an increase in the density of VGAT^{+} puncta (Fig. 3F and G; two-tailed Student's *t*-test $P = 0.0135$). Taken together, these results confirm that the lack of CDKL5 leads to a complex dysregulation of synaptic morphological markers. Excitatory spines are consistently reduced in both the dLGN and in the visual cortex, while V1 shows an additional specific increase in inhibitory connections.

Impaired visual responses in mice with deletion of CDKL5 in cortical excitatory neurons

CDKL5 mutant mice present a deficit in the processing of visual stimuli that can be assessed with a remarkably high discrimination power by IOS imaging of visually evoked responses (22). These abnormal visual responses, however, could arise from defects in upstream visual areas with no intrinsic dysfunction present in visual cortical circuits. In order to assess the specific contribution of the visual cortex, we used a conditional KO mouse model in which the removal of the floxed CDKL5 allele in mutant mice (CDKL5$^{flox/y}$) was achieved by crossing these mice with mice expressing CRE-recombinase driven by the emx1 promoter (emx1-CRE$^{+/-}$). As a result, CDKL5$^{flox/y}$;emx1-CRE$^{+/-}$ animals (cKO) lack CDKL5 only in cortical excitatory neurons and in some glial cells (11), thus sparing all the subcortical visual areas (Supplementary Material, Fig. S4). The expression of CRE-recombinase driven with the emx1 promoter is known to induce recombination as early as at embryonic day (E) 10.5 (11), a time point in which the expression of all the most abundant isoforms of CDKL5 in the mouse brain is still very low (12). This ensures that the phenotypic effects observable in adult mice are the result of an altered development or maturation, closely resembling CDKL5 null mice and patients.

To explore the role of cortical CDKL5 in the pathogenesis of visual deficits in CDKL5 mutants, we first asked whether the morphological alterations previously identified in germline CDKL5 null mice were present in cKO mice in which CDKL5 is normally present in subcortical visual nuclei. Since the retina is unaffected in CDKL5 germline mutants, we began evaluating the presence of such alterations in the visual pathway of cKO mice from the dLGN. Spine density and morphology ($N = 4$ per group), PSD95^{+} puncta ($N = 3$ per group) and VGAT^{+} puncta ($N = 4$ per group) were analyzed in cKO and WT littermates. The results showed that spine density in the dLGN of cKO mice was not different from WT control mice (Fig. 4A; two-tailed Student's *t*-test $P = 0.528$). Moreover, both the proportion of mature and immature spines (Fig. 4B; χ^2 test $P = 0.061$) and their morphology (Fig. 4C; χ^2 test $P = 0.163$) were unaltered. Finally, the density of PSD95^{+} and VGAT^{+} puncta did not differ between WT and cKO mice (Fig. 4D–G; two-tailed Student's *t*-test $P = 0.533$ for PSD95 and $P = 0.812$ for VGAT). Thus, as expected from the pattern of expression of Cre recombinase, the cKO model preserves the integrity of the subcortical retino-cortical pathway, allowing to study the role of cortical CDKL5 in the genesis of visual alterations.

We then asked whether cortical CDKL5 plays a necessary role in the normal physiology of cortical visual processing. To this purpose, we performed IOS imaging, recording visually evoked responses in male cKO animals ($N = 8$) and, as a control, in parental mouse lines expressing CRE ($N = 5$; emx1-CRE$^{+/-}$) or carrying a CDKL5 floxed allele ($N = 9$; CDKL5$^{flox/y}$; Fig. 5C and D). IOS response amplitude to visual stimulation was significantly different between groups [Fig. 5A; one-way analysis of variance (ANOVA) $p = 0.004$]. cKO animals showed a decreased response